crystals

MDPI

Article

Low-Temperature Magnetic and Magnetocaloric Properties of Manganese-Substituted $Gd_{0.5}Er_{0.5}CrO_3$ Orthochromites

Neeraj Panwar [1,*], Kuldeep Singh [1], Komal Kanwar [1], Yugandhar Bitla [1], Surendra Kumar [2] and Venkata Sreenivas Puli [3,4]

[1] Department of Physics, Central University of Rajasthan Bandarsindri, Ajmer 305817, Rajasthan, India; 2019phdph006@curaj.ac.in (K.S.); 2017phdph02@curaj.ac.in (K.K.); bitla@curaj.ac.in (Y.B.)
[2] Department of Physics, Sri Venkateswara College, University of Delhi, Dhaula Kuan, New Delhi 110021, Delhi, India; surendra.kumar@svc.ac.in
[3] National Research Council, Washington, DC 20001, USA; venkata.puli.ctr@us.af.mil
[4] Materials and Manufacturing Directorate, Air Force Research Laboratory, 3005 Hobson Way, Wright Patterson Air Force Base, OH 45433, USA
* Correspondence: neerajpanwar@curaj.ac.in

Abstract: Rare-earth chromites have been envisioned to replace gas-based refrigeration technology because of their promising magnetocaloric properties at low temperatures, especially in the liquid helium temperature range. Here, we report the low-temperature magnetic and magnetocaloric properties of $Gd_{0.5}Er_{0.5}Cr_{1-x}Mn_xO_3$ (x = 0, 0.1, 0.2, 0.3, 0.4 and 0.5) rare-earth orthochromites. The Néel transition temperature (T_N) was suppressed from 144 K for $Gd_{0.5}Er_{0.5}CrO_3$ to 66 K for the $Gd_{0.5}Er_{0.5}Cr_{0.5}Mn_{0.5}O_3$ compound. Furthermore, magnetization reversal was observed in the magnetization versus temperature behavior of the $Gd_{0.5}Er_{0.5}Cr_{0.6}Mn_{0.4}O_3$ and $Gd_{0.5}Er_{0.5}Cr_{0.5}Mn_{0.5}O_3$ compounds at 100 Oe applied magnetic field. The magnetic entropy change ($-\Delta S$) value varied from 16.74 J/kg-K to 7.46 J/kg-K, whereas the relative cooling power (RCP) ranged from 375.94 J/kg to 220.22 J/kg with a Mn ion concentration at 5 T field and around 7.5 K temperature. The experimental results were substantiated by a theoretical model. The present values of the magnetocaloric effect are higher than those of many undoped chromites, manganites and molecular magnets in the liquid helium temperature range.

Keywords: rare-earth orthochromites; magnetization reversal; magnetocaloric effect

Citation: Panwar, N.; Singh, K.; Kanwar, K.; Bitla, Y.; Kumar, S.; Puli, V.S. Low-Temperature Magnetic and Magnetocaloric Properties of Manganese-Substituted $Gd_{0.5}Er_{0.5}CrO_3$ Orthochromites. *Crystals* **2022**, *12*, 263. https://doi.org/10.3390/cryst12020263

Academic Editors: Alessandra Toncelli and Željka Antić

Received: 29 January 2022
Accepted: 12 February 2022
Published: 15 February 2022

1. Introduction

Perovskite materials have been widely recognized for their diverse and intriguing properties, such as magnetic, electrical and photocatalytic, etc. [1–4]. As far as the magnetic properties of various perovskite materials are concerned, rare-earth orthochromites $RCrO_3$ (R = rare-earth ion) exhibit interesting magnetic properties viz. exchange bias [5], spin reorientation [6], magnetization reversal [7–9] and magnetocaloric effect (MCE) [10–13]. It is now a well-established fact that there are three types of magnetic interactions, namely Cr^{3+}-Cr^{3+}, Cr^{3+}-R^{3+} and R^{3+}-R^{3+}, in $RCrO_3$ materials, which govern their distinct magnetic properties in different temperature ranges [5]. The interaction Cr^{3+}-Cr^{3+} is responsible for the canted antiferromagnetic behavior below the Néel transition temperature, whereas the Cr^{3+}-R^{3+} interaction gives rise to negative magnetization or magnetization reversal below a certain temperature, known as the compensation temperature, provided that the R^{3+} ion is magnetic. The negative magnetization occurs due to the antiparallel coupling between the Cr^{3+} moments and rare-earth ion moments [14]. Since the last decade, researchers have also been exploring these materials for their usefulness as a low-temperature refrigerant employing the magnetocaloric effect, which is measured in terms of magnetic entropy change and relative cooling power [10–13,15–20]. Magnetic refrigeration involving solid materials is a cooling technology that is more efficient, inexpensive, safer and more

environmentally friendly than the conventional vapor-compression-based technology. It was reported that Gadolinium and Gadolinium-based compounds are important working materials for magnetic refrigeration. For example, Yin et al. reported 31.6 J/kg-K magnetic entropy change in $GdCrO_3$ single crystal at 3 K under a 4.4 T applied magnetic field [18]. Shi et al. also reported a magnetic entropy change of 27.6 J/kg-K in $Er_{0.33}Gd_{0.67}CrO_3$ at 5 K and 7 T [19]. The effect of Mn substitution at the Cr site in $Gd_{0.5}Er_{0.5}CrO_3$ has not been explored yet. Therefore, it is worthwhile to investigate the magnetic and magnetocaloric properties of Mn-substituted $Gd_{0.5}Er_{0.5}CrO_3$ compounds.

In the present work, we synthesized $Gd_{0.5}Er_{0.5}Cr_{1-x}Mn_xO_3$ (x = 0, 0.1, 0.2, 0.3, 0.4, 0.5) compounds and investigated the effect of Mn substitution on the magnetic and magnetocaloric properties. We also compared the experimental results with theoretical models.

2. Experimental Details

$Gd_{0.5}Er_{0.5}Cr_{1-x}Mn_xO_3$ (x = 0, 0.1, 0.2, 0.3, 0.4, 0.5) (abbreviated as GECMO) orthochromites were prepared by the solid-state reaction method. Stoichiometric amounts of high-purity Gd_2O_3 (99.99%, Sigma Aldrich, St. Louis, MO, USA), Er_2O_3 (99.99%, Sigma Aldrich, St. Louis, MO, USA), Cr_2O_3 (99.99%, Sigma Aldrich, St. Louis, MO, USA) and MnO_2 (99.99%, Sigma Aldrich, St. Louis, MO, USA) were mixed and grounded. The mixed powders were calcined for 24 h at 800 °C and 1100 °C. Finally, the calcined powders were reground and pressed into uniform cylindrical pellets, which were sintered at 1450 °C for 48 h under ambient conditions. The samples were characterized for phase identification using an X-ray diffractometer (XRD; PANalytical-Empyrean, Almelo, The Netherlands) at room temperature using Cu-K_α radiation with wavelength 1.5404 Å at a step of 0.01° per second between 20° and 80°. Magnetic measurements were performed using a physical properties measurement system (PPMS DynaCool). Magnetization temperature data were collected between 2 K and 300 K in field-cooled (FC) and zero-field-cooled (ZFC) modes. The ramp rate was 4K/minute for both the modes. The magnetization–applied field ($M - H$) isotherms were measured under $H = \pm 8$ T.

3. Results and Discussion

3.1. Structural Study

Figure 1 displays the Rietveld-refined XRD patterns of the sintered GECMO orthochromites. It is clear from the XRD patterns that there are no impurity peaks in these series of samples and the diffraction peaks are well matched with the pristine $GdCrO_3$ compound (JCPDS Card No. 25-1056). The refinement was carried out by using Fullprof software with orthorhombic structure and *Pnma* space group. The calculated lattice parameters, unit cell volume (V), reliability factors, octahedral bond length (Cr–O), octahedral tilt angles, strain factor and Goldschmidt tolerance factor (t) of all compounds are presented in Table 1. It can be seen that there was an increase in the lattice constants a and c, while the b value was reduced with increasing Mn^{3+} ion content. Their variation is shown in Figure 2a. Further, the lattice volume was also increased because of the larger ionic radius of the Mn^{3+} ion (0.645 Å) compared to that of the Cr^{3+} ion (0.615 Å) (Figure 2a). When the Mn^{3+} ion was substituted at the Cr^{3+} ion site, a strain developed in the lattice because of the different ionic radii, and, to ensure the stability of the crystal structure, the CrO_6 octahedra rotated or tilted. The strain factor was calculated by $S = 2(a - c)/(a + c)$, which arises as a result of octahedral rotation/tilting [21]. The distortion in the perovskite structure is also represented by the octahedral bond length and tilt angles $\theta_{[101]}$ and $\phi_{[010]}$. In the present study, the octahedral bond length Cr–O and tilt angles $\theta_{[101]}$ and $\phi_{[010]}$ were calculated by the Zhao formalism [22] as follows:

$$\text{Cr–O} = \left(\frac{ab}{4c}\right),\ \theta_{[101]} = \cos^{-1}\left(\frac{c}{a}\right) \text{ and } \phi_{[010]} = \cos^{-1}\left(\frac{\sqrt{2}c}{b}\right)$$

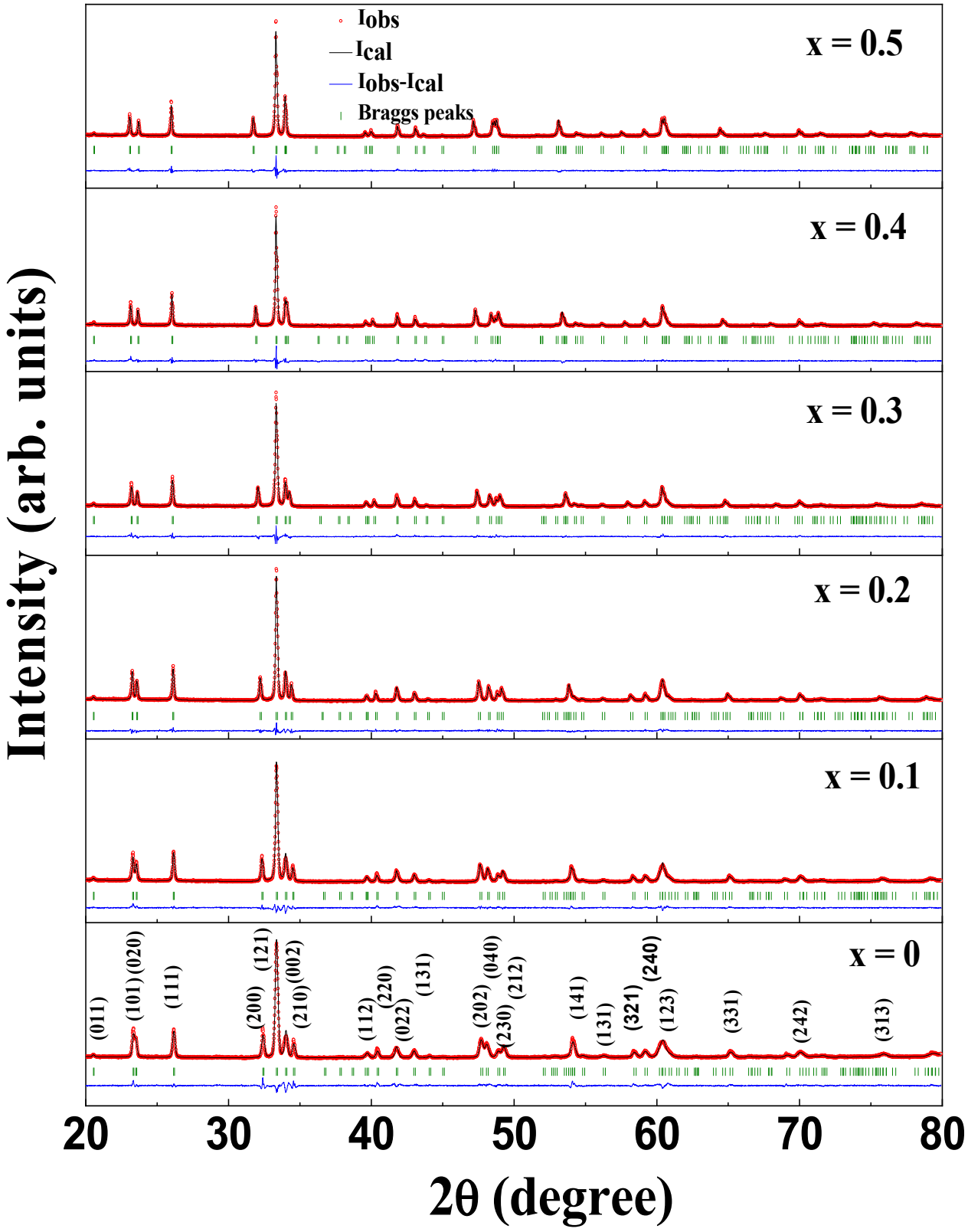

Figure 1. Rietveld-refined XRD patterns of the GECMO series.

Table 1. Lattice parameters, unit cell volume (V), reliability factors, octahedral bond length, tilt angles, strain factor and Goldschmidt tolerance factor (t) of GECMO series.

	$x = 0$	$x = 0.1$	$x = 0.2$	$x = 0.3$	$x = 0.4$	$x = 0.5$
a (Å)	5.5220	5.5335	5.5530	5.5835	5.6072	5.6372
b (Å)	7.5648	7.5541	7.5439	7.5376	7.5183	7.5029
c (Å)	5.2691	5.2709	5.2721	5.2767	5.2740	5.2744
V (Å^3)	220.109	220.330	220.860	222.081	222.340	223.085
χ^2 (%)	3.29	2.48	2.08	1.94	2.62	2.03
R_P (%)	19	16.7	16.1	16.7	19.5	19.2
R_{WP} (%)	14.9	12.6	11.4	11.7	13.6	12.8
Cr–O (Å)	1.982	1.9825	1.9864	1.9925	1.9983	2.0047
θ (°)	17.40	17.71	18.29	19.06	19.84	20.65
ϕ (°)	9.922	9.32	8.75	8.06	7.22	6.19
S	0.0468	0.0486	0.0518	0.0564	0.0612	0.0665
t	0.8523	0.8510	0.8497	0.8484	0.8472	0.8459

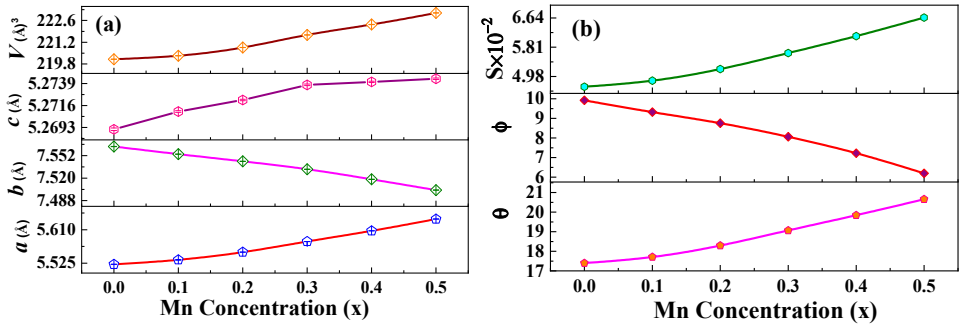

Figure 2. (**a**) Lattice parameters, volume, (**b**) strain parameter and tilt angle variation as a function of Mn concentration.

The octahedral bond length Cr–O increased in Mn-substituted compounds because the Mn^{3+} ion had a larger ionic radius than the Cr^{3+} ion. The rotation of the CrO_6 octahedron occurred in both planes, i.e., in-plane (along a and c axis) and out-of-plane (along b axis). The tilt angle $\theta_{[101]}$ was found to increase, while the rotational angle $\phi_{[010]}$ decreased with an increase in the Mn^{3+} ion concentration (Figure 2b). In determining the stability of the perovskite structure, the Goldschmidt tolerance factor (t) plays a key role. In order to calculate the tolerance factor (t) for the present compounds, we used the formula $t = <\mathrm{Gd/Er–O}>/\sqrt{2} <\mathrm{Cr/Mn–O}>$. The unity value of t corresponds to an ideal perovskite structure, while $0.75 \leq t \leq 0.9$ favors a distorted orthorhombic structure [23,24]. Further, it should also be noted that the classical consideration of ionic size alone cannot explain the structural characteristics. To obtain a more accurate understanding of the structural characteristics when Mn^{3+} ions replace Cr^{3+} ions, we performed a detailed structural analysis. Figure 3a presents the crystal structure of the GECO compound generated using VESTA software. It can be noticed that the structure is distorted from the ideal cubic structure (distortion shown in Figure 3b). This results in variation in the bond lengths. Figure 3c shows the Cr–O bond length variation in the Cr–O_6 octahedron as a function of the Mn concentration. The difference among the three Cr–O bond lengths in all compounds can be correlated with the Jahn–Teller (JT) distortion of Mn^{3+} ions, along with a contribution from intrinsic structural distortion. The in-plane (orthorhombic-like) and out-of-plane (tetragonal-like) distortions evaluated by Q_2 [$= l_y - l_x$], and Q_3 [$= (2 \times l_z - l_x - l_y)/\sqrt{3}$], respectively, are shown in Figure 3d. Here, l_x, l_y and l_z denote the long and short Cr–O_2 bond lengths mainly in the ac plane and the middle bond length Cr–O_1 mainly along the b axis (out of plane), respectively. O_1 and O_2 stand for the apical and equatorial oxygen atoms. Here, the large and positive magnitude of Q_2 is associated with the Jahn–Teller distortion and the low and negative value of Q_3 indicates that an out-of-plane distortion along the c

axis is competing with the JT distortion [25,26]. This implies that the lattice deformation is primarily confined to the *ac* plane. A higher value of Q_2 in comparison to Q_3 indicates a decrease in the *b* lattice parameter value and an increase in the *a* and *c* parameters, as shown in Figure 2a. The continuous variation in the in-plane and out-of-plane distortions with Mn substitution should have an impact on the magnetic properties.

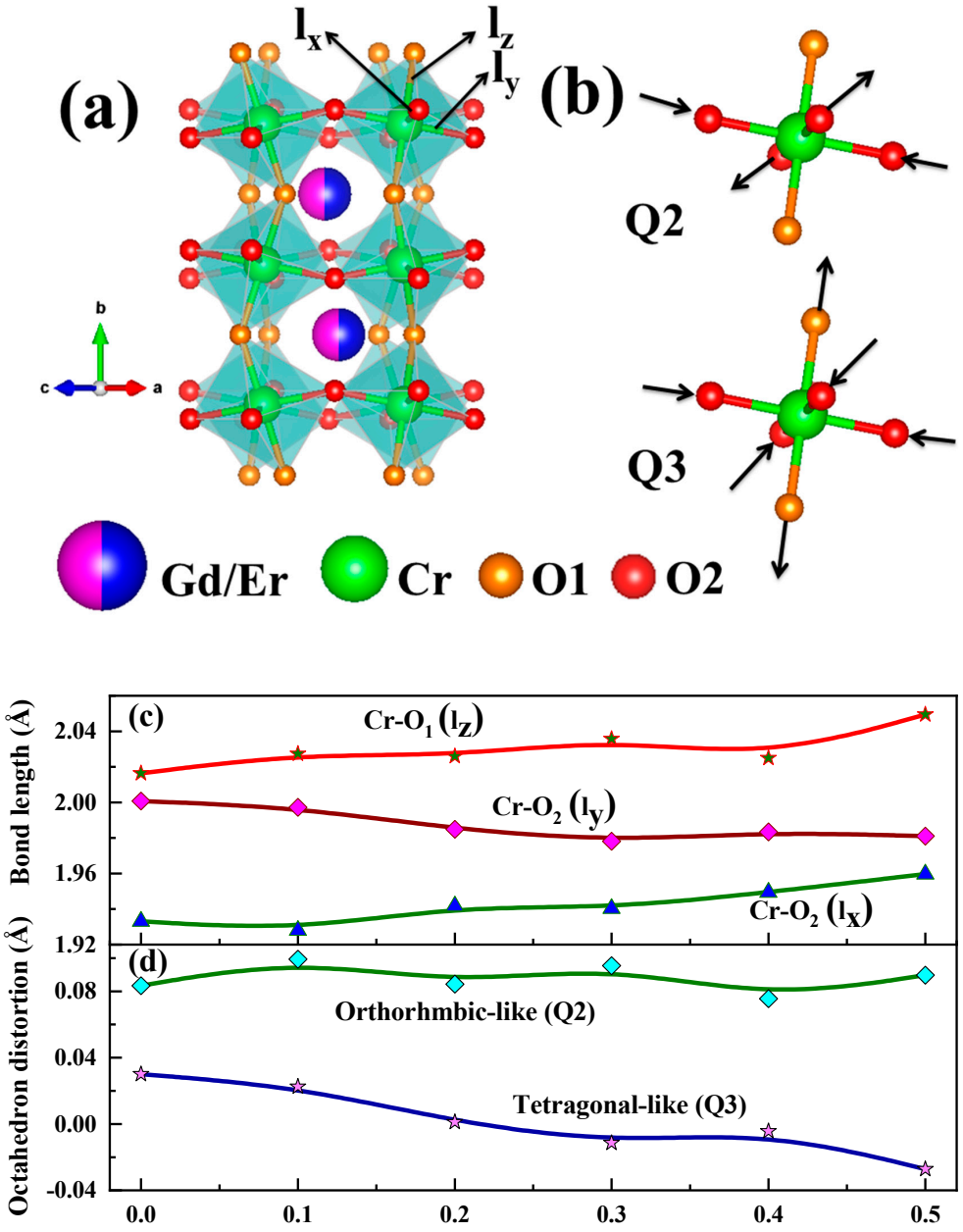

Figure 3. (**a**) Crystal structure of $Gd_{0.5}Er_{0.5}CrO_3$ compound obtained from the VESTA software; l_x, l_y and l_z denote the long and short Cr– O_2 bond lengths mainly in the *ac* plane and the middle length Cr–O_1 mainly along the *b* axis (out of plane), respectively. (**b**) Q_2 and Q_3 represent the orthogonal-like and tetragonal-like distortions, respectively. (**c**) Bond lengths and (**d**) octahedral distortion variation as a function of Mn concentration.

3.2. Magnetic Study

The zero-field-cooled (ZFC) and field-cooled (FC) magnetization plots of the GECMO series as a function of temperature from 2 K to 300 K at 100 Oe applied magnetic field are shown in Figure 4a–f. Above T_N (i.e., the Néel transition temperature), both the FC and ZFC curves possess almost identical magnetization, whereas the curves become bifurcated below

T_N. The canted antiferromagnetism of Cr^{3+} ions may be responsible for this bifurcation. The transition temperature for the pristine (x = 0) sample at 100 Oe magnetic field is ~144 K, which was evaluated by the first-order derivative of the magnetization temperature curve. The transition temperature decreased with an increase in Mn^{3+} ion content. The decrease in T_N was due to the weakening of the AFM interaction between Cr^{3+} ions and the development of ferromagnetic double-exchange interaction Cr^{3+}-Mn^{3+} via the O^{2-} ion. It can be seen that, below T_N, magnetization in both modes (ZFC and FC) increased to a certain value with the lowering of temperature. It attained the maximum value below 10 K, corresponding to the ordering of rare-earth Gd^{3+} and Er^{3+} ions, and after this, it started decreasing. The magnetization increased with Mn^{3+} ion doping for the samples with x = 0, 0.1, 0.2, 0.3 in FC mode, but it decreased in the case of the samples with higher Mn content. The magnetization in both modes (FC and ZFC) passed the zero magnetization and became negative for the two samples with x = 0.4 and 0.5. The temperature where the magnetization crosses the temperature axis (M = 0) is known as the compensation temperature (T_{comp}). Further, in the case of the compound with x = 0.4, magnetization again started increasing below 10 K. This may have been due to the rotation of the net magnetic moment from one easy direction to the other. In the present study, it is likely that a higher concentration of manganese was responsible for the creation of a negative internal field that rotated the magnetization of Gd^{3+} and Er^{3+} ions in the opposite direction of the magnetization of Cr^{3+} ions. As we shall see later, the calculated value of the internal field was negative (i.e., opposite to magnetization of Cr^{3+} ions) for compounds with x = 0.4 and 0.5.

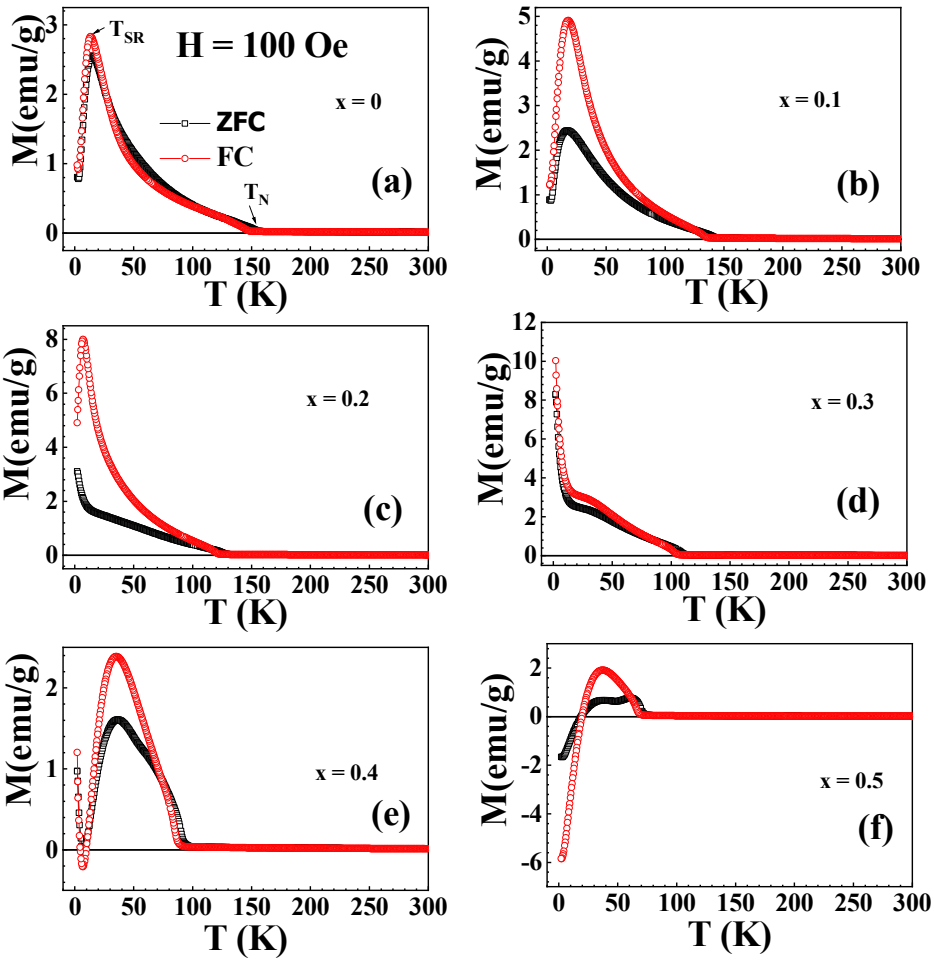

Figure 4. (**a**–**f**): ZFC and FC magnetization curves of GECMO series measured under 100 Oe magnetic field.

Figure 5a–d demonstrate the zero-field-cooled and field-cooled magnetization as a function of temperature from 2 K to 300 K for the compound with x = 0.5 at 500 Oe, 1 kOe, 2.5 kOe and 5 kOe applied magnetic field. Here, we observed that, for a higher magnetic field, negative magnetization disappeared. This means that the applied field of these values dominated the internal field, so the overall magnetization became positive because of the flipping of the magnetization of Gd^{3+}/Er^{3+} ions in the direction of the applied field.

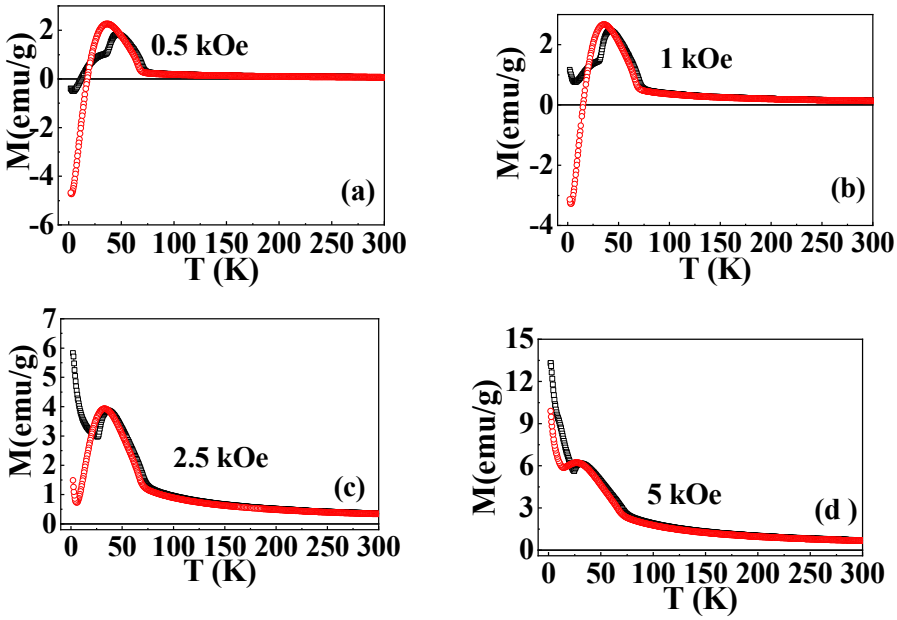

Figure 5. (**a**–**d**): ZFC and FC magnetization curves of x = 0.5 compound measured under 500 Oe, 1 kOe, 2.5 kOe and 5 kOe magnetic field.

Further, the FC magnetization data of the compounds, in which negative magnetization appeared, were fitted using the following equation [27]:

$$M = M_{\mathrm{Cr}} + \frac{C(H + H_I)}{(T - \theta)} \quad (1)$$

In Equation (1), M is the total magnetization, M_{Cr} is the magnetization of canted Cr^{3+} ions, C is the Curie constant, H_I is the internal field due to Cr^{3+} ions, H is the applied field and θ is the Weiss temperature. The fitting is shown by a solid red line in Figure 6a,b. The obtained parameters are listed in Table 2. We found negative values of internal field (H_I) for these compounds, which support the notion that induced magnetization occurred in the opposite direction to the applied field.

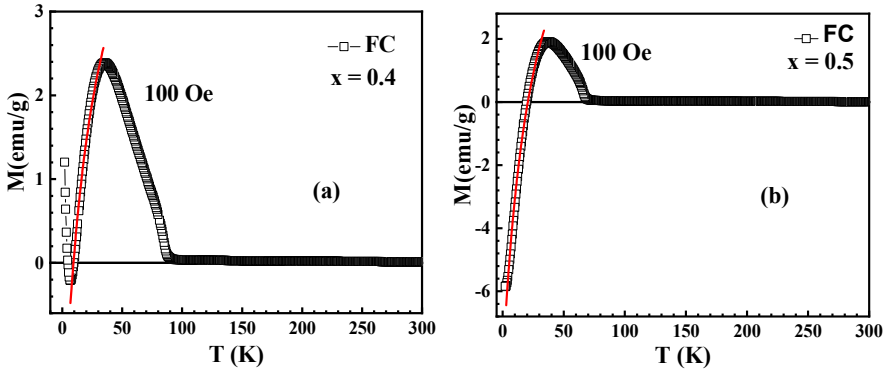

Figure 6. (**a**,**b**): The FC magnetization curves fitted to Equation (1) for compounds with x = 0.4 and x = 0.5 measured under 100 Oe magnetic field.

Table 2. List of fitting parameters for negative magnetization of *M*–*T* curves in FC mode as shown in Figure 6a,b.

Compound	External Field (Oe)	H_I (Oe)	θ (K)
$x = 0.4$	100	−301.81	−24.43
$x = 0.5$	100	−360.70	−24.59

Figure 7a–f express the inverse of magnetic susceptibility (χ^{-1}) versus temperature (T) plots of GECMO compounds measured at 100 Oe applied magnetic field. In the high-temperature region, the inverse of magnetic susceptibility obeys the Curie–Weiss law $\chi = C/(T\text{-}\theta)$, where C is the Curie constant and θ is the Weiss temperature. The solid red line shows the fitted curve using the Curie–Weiss law in the paramagnetic region above the transition temperature. The experimental value of the effective magnetic moment was calculated in the unit of Bohr magneton (μ_B) using the fitted Curie constant (C) value by the following equation [28]:

$$\mu_{\text{eff}}^{exp.} = \sqrt{\frac{3K_B\,C}{N}} = \sqrt{8c} \tag{2}$$

where N is the Avogadro number and k_B is the Boltzmann constant. The theoretical effective magnetic moment value was also estimated using the free ionic moments of Gd^{3+} (7.9 μ_B), Er^{3+} (9.59 μ_B), Cr^{3+} (3.87 μ_B) and Mn^{3+} (4.90 μ_B) by the following equation:

$$\mu_{\text{eff}}^{Th.} = \sqrt{(0.5)\left(\mu_{\text{eff}}^{Gd}\right)^2 + (0.5)\left(\mu_{\text{eff}}^{Er}\right)^2 + (1-x)\left(\mu_{\text{eff}}^{Cr}\right)^2 + x\left(\mu_{\text{eff}}^{Mn}\right)^2} \tag{3}$$

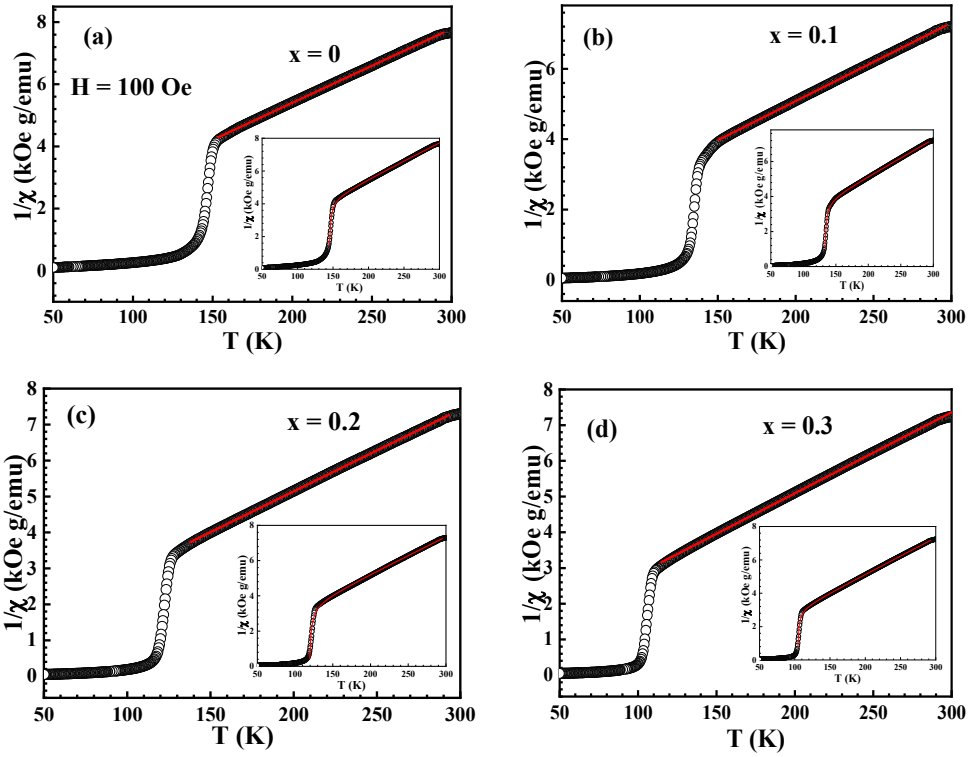

Figure 7. *Cont.*

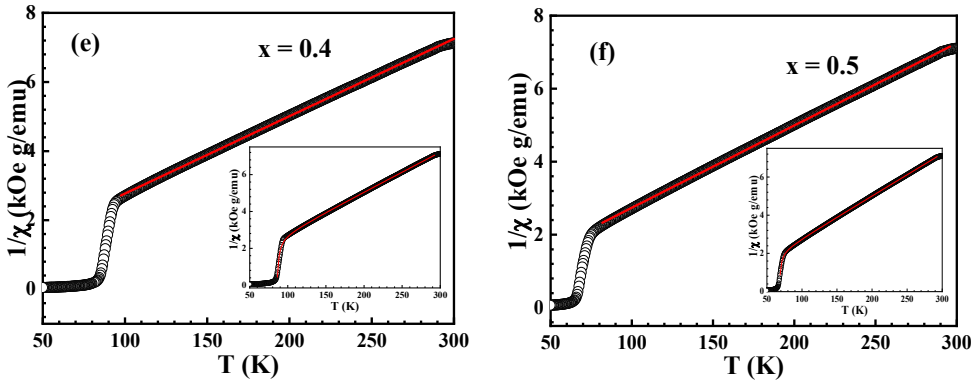

Figure 7. (**a**–**f**): Inverse magnetic susceptibility versus temperature plots of GECMO series measured at 100 Oe applied magnetic field. Open circles represent the experimental data points whereas solid lines of plot display the fitting to the Curie–Weiss law. Insets represent the fitting of inverse magnetic susceptibility versus temperature using Equation (4).

The value of fitted parameters (C and θ) and effective magnetic moment (calculated and experimental) are summarized in Table 3 for all compounds. Here, a negative value of θ suggests that the interaction is antiferromagnetic [29]. It is quite satisfactory that both the values of effective magnetic moment (calculated and experimental) match fairly well with each other.

Table 3. Magnetic parameters: Curie constant C (emu-K/Oe-mole), Weiss temperature θ (K), experimental and theoretical effective magnetic moment obtained from Curie–Weiss fitting, and $T_N^{Cr'}$ (K), θ' (K), C' (emu-K/Oe-mole), fitting parameter T_0 (K) and symmetric and antisymmetric exchange constant obtained from modified Curie–Weiss fitting of inverse susceptibility vs. temperature data.

Compound	x = 0	x = 0.1	x = 0.2	x = 0.3	x = 0.4	x = 0.5
θ (K)	−26.59	−28.57	−26.29	−24.39	−23.73	−21.48
C(emu-K/Oe-mole)	10.99	11.80	11.56	11.59	11.76	11.70
$\mu_{eff}^{exp.}(\mu_B)$	9.38	9.72	9.62	9.63	9.70	9.68
$\mu_{eff}^{Th.}(\mu_B)$	9.60	9.65	9.69	9. 74	9.79	9.83
$T_N^{Cr'}$ (K)	144.28	132.77	119.10	103.91	86.02	68.01
T_0 (K)	143.03	131.33	117.13	102.68	84.23	66.71
θ' (K)	−53.42	−48.98	−51.07	−36.70	−36.8	−28.34
C'(emu-K/Oe-mole)	11.91	12.50	12.41	12.00	12.19	11.91
J_e/k_B	9.54	8.76	7.81	6.85	5.62	4.53
D_e/k_B	2.53	2.60	2.88	2.13	2.33	1.80

As is apparent from Figure 7a–f, the $1/\chi$ versus T data fit well with the Curie–Weiss law above the transition temperature (T_N) and it deviates close to T_N as there is an abrupt drop in $1/\chi$ with temperature reduction. The reason for this is that our samples were in a canted antiferromagnetic state instead of simple antiferromagnetic. Such a deviation from the Curie–Weiss behavior can be accounted for by the antisymmetric exchange (DM) interaction [30]. Thus, the susceptibility was fitted by the modified Curie–Weiss law obtained from the DM interaction:

$$\chi = \frac{C'}{(T-\theta')} \frac{(T-T_0)}{\left(T-T_N^{Cr'}\right)}, \tag{4}$$

where T_0 and $T_N^{Cr'}$ are the fitted parameters, which can be calculated by the formula given by Moriya [30]:

$$T_0 = \frac{2J_e\, ZS(S+1)}{3k_B}, \tag{5}$$

$$T_N^{Cr} = T_0 \left[1 + \left(\frac{D_e}{2\,J_e}\right)^2\right]^{1/2} \quad (6)$$

where Z is the coordination number of Cr^{3+} ions, S is the spin quantum number of Cr^{3+} ions, and J_e and D_e are the strength of symmetric and antisymmetric exchange interactions between Cr^{3+} and Cr^{3+} ions, respectively. The data fitted using Equation (4) are shown as the insets of Figure 7. The fitted parameters C', θ', T_0 and $T_N^{Cr'}$ are summarized in Table 3. The non-zero values of D_e imply the presence of a DM interaction in these compounds.

3.3. Magnetocaloric Study

With the aim of exploring the efficiency of the materials for magnetic refrigeration applications, the isothermal magnetization $M - H$ curves of the GECMO samples were obtained in the first quadrant with an applied field of up to 8 T. Figure 8a–f show the $M - H$ curves obtained from 5 K to 170 K with an interval of 5 K for GECMO samples. There are two criteria that are used to characterize the magnetocaloric effect: the first is the magnetic entropy change (ΔS) and the other is the relative cooling power (RCP). The magnetic entropy change was calculated by using the following Maxwell's relation [31]:

$$\Delta S(\mathrm{T})\Delta_H = \int_{H_I}^{H_F} \left(\frac{\partial M(T,\ H)}{H}\right) dH \quad (7)$$

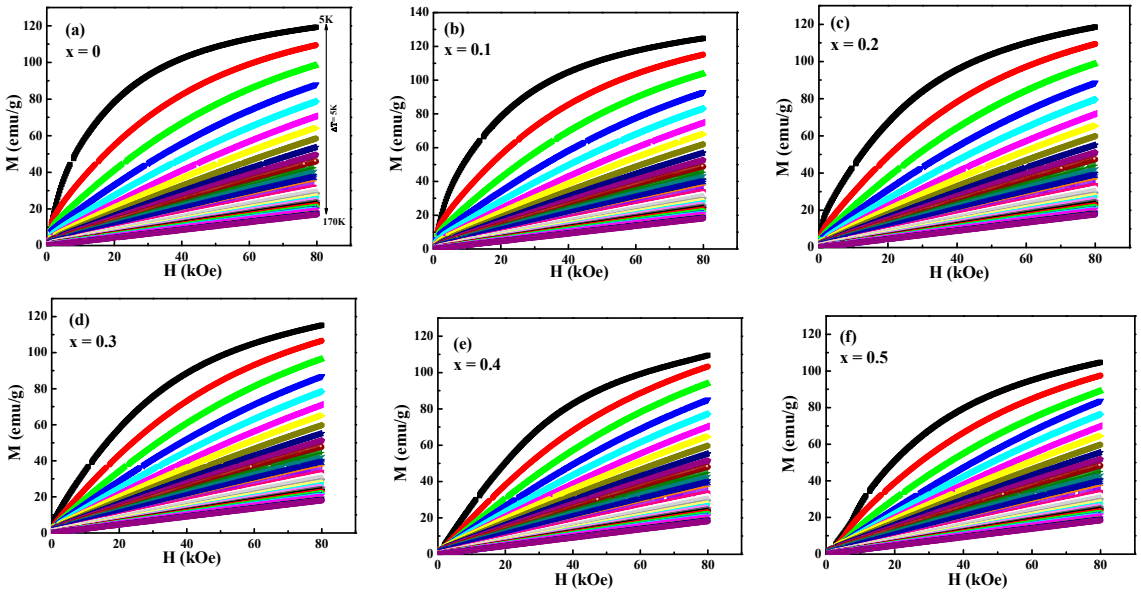

Figure 8. (**a**–**f**): Isothermal magnetization M–H curves of the GECMO series.

Figure 9a–f display the magnetic entropy change calculated from Equation (7) as a function of temperature under various applied field strengths. It can be noticed that the value of $-\Delta S$ increased rapidly with a decrease in temperature. The maximum value of $-\Delta S$ is 26.78 J $Kg^{-1}K^{-1}$ at 7.5 K and at 8 T applied field for the x = 0 compound. This is comparable to the $Er_{0.33}Gd_{0.67}CrO_3$ compound [19] and higher than other compounds such as $DyCrO_3$, $HoCrO_3$, $ErCrO_3$, etc., and dysprosium acetate tetrahydrate [32]. Furthermore, with the Mn doping in the pristine compound, the value of $-\Delta S$ decreased. RCP was evaluated by the following equation

$$\mathrm{RCP} = \int_{T_1}^{T_2} \Delta S(T)_{\Delta H} dT \quad (8)$$

where T_1 and T_2 are the lower and higher temperature of the refrigeration cycle (T_1 = 7.5 K and T_2 = 172.5 K in this study), respectively. A greater RCP value generally denotes a better magnetocaloric compound because of its high cooling efficiency. As displayed in the inset of Figure 9a–f, the value of RCP increased with the increase in applied field. The values of $-\Delta S$ and RCP for the GECMO series are listed in Table 4 for different applied magnetic field values.

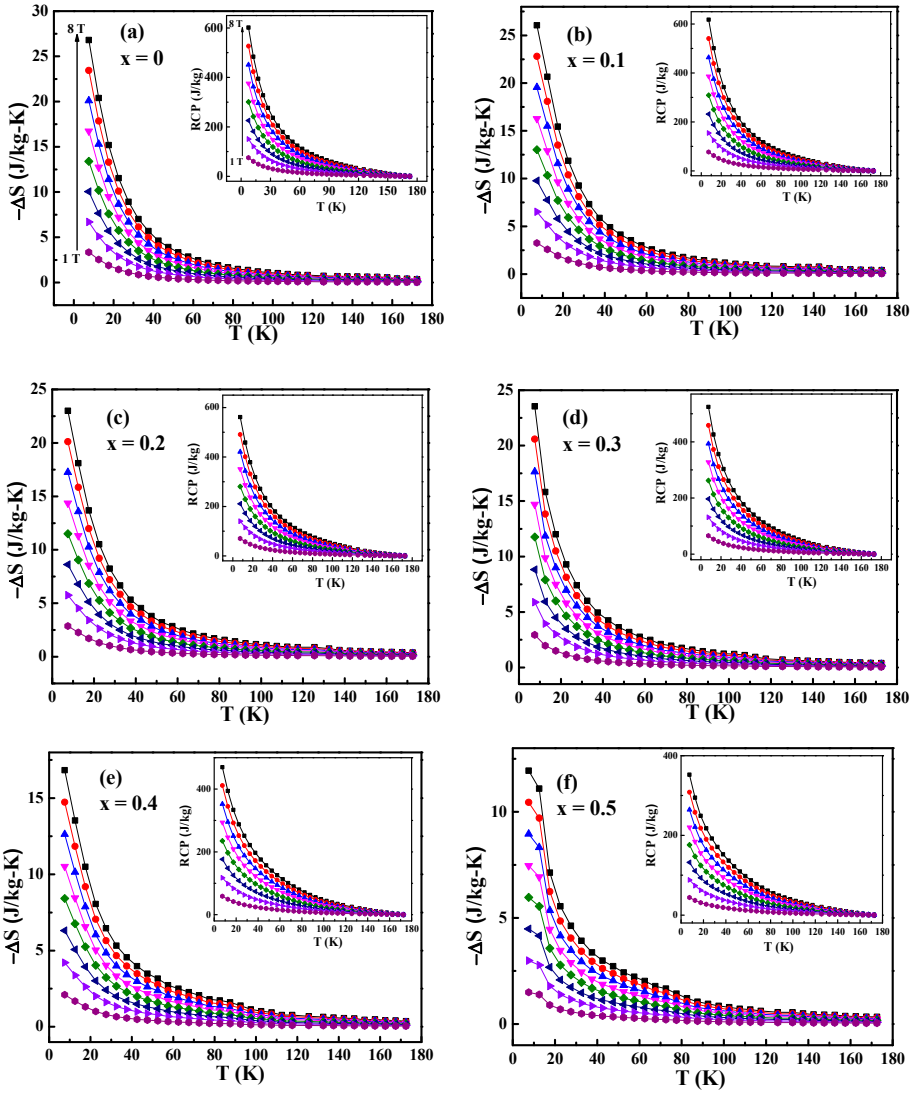

Figure 9. (**a**–**f**): The temperature dependence of magnetic entropy change ($-\Delta S$) and relative cooling power (inset) of GECMO series in magnetic fields up to 8 T.

Table 4. Magnetic entropy change ($-\Delta S$) and relative cooling power (RCP) at different applied magnetic fields for the $Gd_{0.5}Er_{0.5}Cr_{1-x}Mn_xO_3$ series.

Compound	$x = 0$		$x = 0.1$		$x = 0.2$		$x = 0.3$		$x = 0.4$		$x = 0.5$	
$H_{Max.}$ (T)	$-\Delta S_{Max.}$ (J/kg-K)	RCP (J/kg)	$-\Delta S_{Max.}$ (J/kg-K)	RCP (J/kg)	$-\Delta S_{Max.}$ (J/kg-K)	RCP (J/kg)	$-\Delta S_{Max.}$ (J/kg-K)	RCP (J/kg)	$-\Delta S_{Max.}$ (J/kg-K)	RCP (J/kg)	$-\Delta S_{Max.}$ (J/kg-K)	RCP (J/kg)
1	3.34	75.18	3.25	77.19	2.87	70.15	2.94	65.52	2.10	58.73	1.49	44.04
2	6.69	150.37	6.51	154.38	5.74	140.30	5.88	131.04	4.20	117.46	2.98	88.09
3	10.04	225.56	9.77	231.57	8.62	210.46	8.82	196.56	6.31	176.20	4.47	132.13
4	13.39	300.75	13.02	308.76	11.49	280.61	11.76	262.08	8.41	234.93	5.96	176.18
5	16.74	375.94	16.28	385.95	14.36	350.76	14.70	327.61	10.52	293.67	7.46	220.22
6	20.09	451.13	19.54	463.14	17.24	420.92	17.64	393.13	12.62	352.40	8.95	264.27
7	23.44	526.32	22.79	540.33	20.11	491.07	20.58	458.65	14.72	411.13	10.44	308.32
8	26.78	601.51	26.05	617.52	22.99	561.23	23.53	524.17	16.83	469.87	11.93	352.36

To gain a better understanding of the magnetocaloric effect, we further explored the magnetic entropy change ($-\Delta S$) in view of the magneto-elastic coupling and electron interaction according to the Landau theory of phase transition [33,34]. According to this, the Gibbs free energy can be defined as:

$$G(T, M) = \frac{1}{2}AM^2 + \frac{1}{4}BM^4 + \frac{1}{6}CM^6 - MH \quad (9)$$

where A, B and C are the temperature-dependent parameters (Landau coefficients). At equilibrium, energy should be minimized, i.e., $\frac{\partial G}{\partial M} = 0$, and Equation (9) gives

$$\frac{H}{M} = \mathrm{A} + BM^2 + CM^4 \quad (10)$$

The Landau coefficients were calculated from the Arrott's plots (H/M vs. M^2) by the best fit method. Magnetic entropy change was obtained by differentiating Gibbs free energy with respect to temperature:

$$\Delta S_M(T, H) = -\frac{1}{2}\frac{\partial A}{\partial T}M^2 - \frac{1}{4}\frac{\partial B}{\partial T}M^4 - \frac{1}{6}\frac{\partial C}{\partial T}M^6 \quad (11)$$

The magnetic entropy change calculated by Landau theory was compared with that calculated by Maxwell's thermodynamic relations under 5 T magnetic field and the comparison is shown in Figure 10a–f. The variation in the Landau coefficients is also shown in the inset of each plot. It can be seen from the plots that the magnetic entropy change versus temperature behavior is the same according to different models.

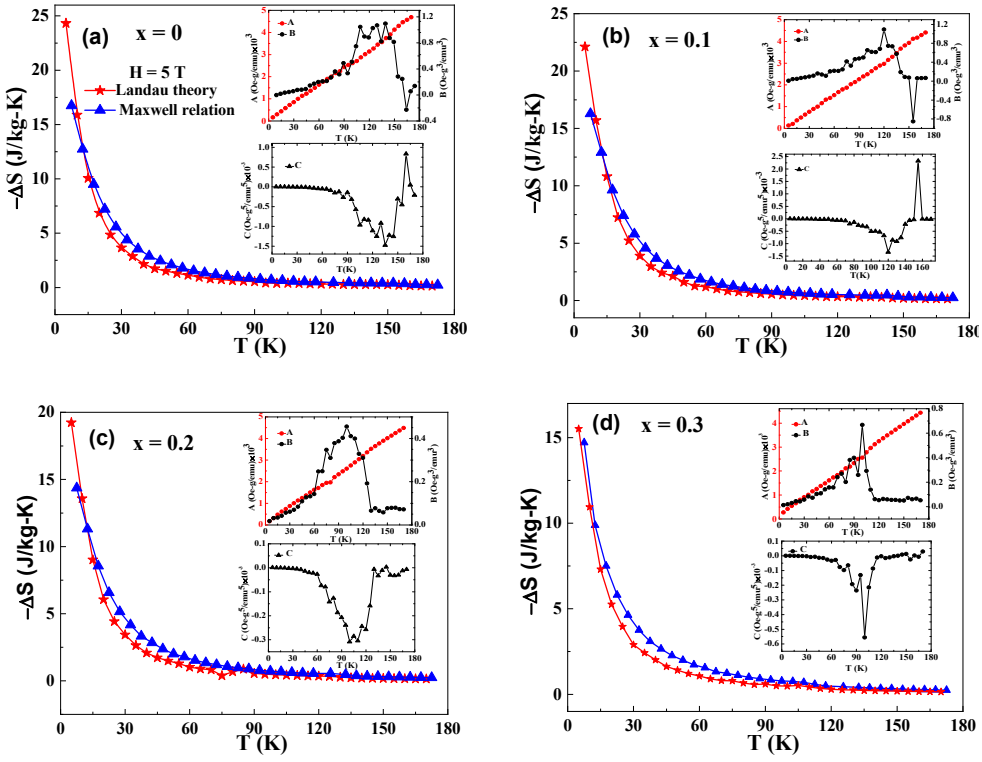

Figure 10. *Cont.*

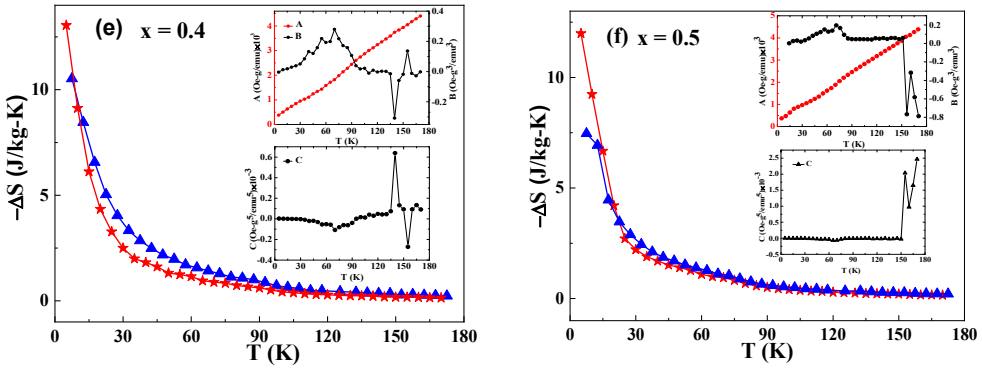

Figure 10. (**a**–**f**): Temperature dependence of magnetic entropy change ($-\Delta S$) of GECMO series calculated using Landau theory and Maxwell's relation. Insets show the variation in Landau coefficients.

4. Conclusions

In this paper, we studied $Gd_{0.5}Er_{0.5}Cr_{1-x}Mn_xO_3$ (x = 0, 0.1, 0.2, 0.3, 0.4, 0.5) compounds for their low-temperature magnetic and magnetocaloric properties. The M–T measurements indicate that the transition temperature for the pristine sample was ~144 K, which decreased with Mn substitution. We also observed negative magnetization at lower magnetic fields in compounds with x = 0.4 and 0.5 Mn concentrations. The existence of the magnetization reversal offers the characteristic switching of magnetization. The magnetocaloric parameters such as magnetic entropy change ($-\Delta S$) varied from 16.74 J/kg-K to 7.46 J/kg-K and relative cooling power (RCP) from 375.94 J/kg to 220.22 J/kg with Mn concentration under a 5 T field change. These values are significant for these materials to be useful as low-temperature magnetic refrigerants, especially below 10 K.

Author Contributions: Conceptualization, N.P.; methodology, N.P.; validation, N.P.; formal analysis, K.S.; investigation, K.S., N.P., Y.B.; resources, S.K.; writing—original draft preparation K.S., K.K., V.S.P.; original draft correct N.P., Y.B. All authors have read and agreed to the published version of the manuscript.

Funding: The research was funded by DST SERB, New Delhi, India through grant No. ECR/2017/002681.

Institutional Review Board Statement: Not applicable.

Informed Consent Statement: Not applicable.

Data Availability Statement: Not applicable.

Acknowledgments: The authors are thankful to the low-temperature high-magnetic-field facility of CURAJ for the magnetic measurements. Neeraj Panwar would like to thank DST SERB, New Delhi, UGC DAE CSR Mumbai and IUAC New Delhi for the grants through Projects ECR/2017/002681, CRS-M-298 and UFR-62317, respectively. V.S.P. acknowledges the National Research Council (NRC) senior research associate fellowship program.

Conflicts of Interest: The authors declare no conflict of interest.

References

1. Ateia, E.E.; Ismail, H.; Elshimy, H.; Abdelmaksoud, M.K. Structural and Magnetic Tuning of $LaFeO_3$ Orthoferrite Substituted Different Rare Earth Elements to Optimize Their Technological Applications. *J. Inorg. Organomet. Polym. Mater.* **2021**, *31*, 1713–1725. [CrossRef]
2. Chakraborty, P.; Basu, S. Structural, electrical and magnetic properties of Er doped $YCrO_3$ nanoparticles. *Mater. Chem. Phys.* **2021**, *259*, 124053. [CrossRef]
3. Yoshii, K. Magnetic properties of perovskite $GdCrO_3$. *J. Solid State Chem.* **2001**, *159*, 204–208. [CrossRef]
4. Aamir, M.; Bibi, I.; Ata, S.; Majid, F.; Kamal, S.; Alwadai, N.; Sultan, M.; Iqbal, S.; Aadil, M.; Iqbal, M. Graphene oxide nanocomposite with Co and Fe doped $LaCrO_3$ perovskite active under solar light irradiation for the enhanced degradation of crystal violet dye. *J. Mol. Liq.* **2021**, *322*, 114895. [CrossRef]
5. Wang, L.; Wang, S.W.; Zhang, X.; Zhang, L.L.; Yao, R.; Rao, G.H. Reversals of magnetization and exchange-bias in perovskite chromite $YbCrO_3$. *J. Alloys Compd.* **2016**, *662*, 268–271. [CrossRef]

6. Hornreich, R.M. Magnetic interactions and weak ferromagnetism in the rare-earth orthochromites. *J. Magn. Magn. Mater.* **1978**, *7*, 280–285. [CrossRef]
7. Su, Y.; Zhang, J.; Feng, Z.; Li, L.; Li, B.; Zhou, Y.; Chen, Z.; Cao, S. Magnetization reversal and Yb^{3+}/Cr^{3+} spin ordering at low temperature for perovskite $YbCrO_3$ chromites. *J. Appl. Phys.* **2010**, *108*, 013905. [CrossRef]
8. Cao, Y.; Cao, S.; Ren, W.; Feng, Z.; Yuan, S.; Kang, B.; Lu, B.; Zhang, J. Magnetization switching of rare earth orthochromite $CeCrO_3$. *Appl. Phys. Lett.* **2014**, *104*, 232405. [CrossRef]
9. Panwar, N.; Joby, J.P.; Kumar, S.; Coondoo, I.; Vashundhara, M.; Kumar, N.; Palai, R.; Singhal, R.; Katiyar, R.S. Observation of magnetization reversal behavior in $Sm_{0.9}Gd_{0.1}Cr_{0.85}Mn_{0.15}O_3$ orthochromites. *AIP Adv.* **2018**, *8*, 055818. [CrossRef]
10. Yin, S.; Sharma, V.; McDannald, A.; Reboredo, F.A.; Jain, M. Magnetic and magnetocaloric properties of iron substituted holmium chromite and dysprosium chromite. *RSC Adv.* **2016**, *6*, 9475–9483. [CrossRef]
11. Sharma, M.K.; Mukherjee, K. Magnetic and universal magnetocaloric behavior of rare-earth substituted $DyFe_{0.5}Cr_{0.5}O_3$. *J. Magn. Magn. Mater.* **2017**, *444*, 178–183. [CrossRef]
12. Yin, S.; Seehra, M.S.; Guild, C.J.; Suib, S.L.; Poudel, N.; Lorenz, B.; Jain, M. Magnetic and magnetocaloric properties of $HoCrO_3$ tuned by selective rare-earth doping. *Phys. Rev. B* **2017**, *95*, 184421. [CrossRef]
13. Zhang, H.; Qian, H.; Xie, L.; Guo, Y.; Liu, Y.; He, X. The spin reorientation and improvement of magnetocaloric effect in $HoCr_{1-x}Ga_xO_3$ ($0 \leq x \leq 0.5$). *J. Alloys Compd.* **2021**, *885*, 160863. [CrossRef]
14. Yoshii, K. Positive exchange bias from magnetization reversal in $La_{1-x}Pr_xCrO_3$ ($x \sim 0.7$–0.85). *Appl. Phys. Lett.* **2011**, *99*, 142501. [CrossRef]
15. Oliveira, G.N.P.; Machado, P.; Pires, A.L.; Pereira, A.M.; Araújo, J.P.; Lopes, A.M.L. Magnetocaloric effect and refrigerant capacity in polycrystalline $YCrO_3$. *J. Phys. Chem. Solids* **2016**, *91*, 182–188. [CrossRef]
16. Oliveira, G.N.P.; Pires, A.L.; Machado, P.; Pereira, A.M.; Araújo, J.P.; Lopes, A.M.L. Effect of chemical pressure on the magnetocaloric effect of perovskite-like $RCrO_3$ (R-Yb, Er, Sm and Y). *J. Alloys Compd.* **2019**, *797*, 269–276. [CrossRef]
17. Kumar, S.; Coondoo, I.; Vasundhara, M.; Kumar, S.; Kholkin, A.L.; Panwar, N. Structural, magnetic, magnetocaloric and specific heat investigations on Mn doped $PrCrO_3$ orthochromites. *J. Phys. Condens. Matter* **2017**, *29*, 195802. [CrossRef]
18. Yin, L.H.; Yang, J.; Kan, X.C.; Song, W.H.; Dai, J.M.; Sun, Y.P. Giant magnetocaloric effect and temperature induced magnetization jump in $GdCrO_3$ single crystal. *J. Appl. Phys.* **2015**, *117*, 133901. [CrossRef]
19. Shi, J.; Yin, S.; Seehra, M.S.; Jain, M. Enhancement in magnetocaloric properties of $ErCrO_3$ via A-site Gd substitution. *J. Appl. Phys.* **2018**, *123*, 193901. [CrossRef]
20. Kanwar, K.; Coondoo, I.; Anas, M.; Malik, V.K.; Kumar, P.; Kumar, S.; Kulriya, P.K.; Kaushik, S.D.; Panwar, N. A comparative study of the structural, optical, magnetic and magnetocaloric properties of $HoCrO_3$ and $HoCr_{0.85}Mn_{0.15}O_3$ orthochromites. *Ceram. Int.* **2021**, *47*, 7386–7397. [CrossRef]
21. Chan, T.S.; Liu, R.S.; Yang, C.C.; Li, W.-H.; Lien, Y.H.; Huang, C.Y.; Lee, J.F. Chemical Size Effect on the Magnetic and Electrical Properties in the $(Tb_{1-x}\ Eu_x)MnO_3 (0 \leq x \leq 1.0)$ System. *J. Phys. Chem. B* **2007**, *111*, 2262–2267. [CrossRef] [PubMed]
22. Zhao, Y.; Weidner, D.J.; Parise, J.B.; Cox, D.E. Thermal expansion and structural distortion of perovskite-data for $NaMgF_3$ perovskite. Part I. *Phys. Earth Planet. Inter.* **1993**, *76*, 1–16. [CrossRef]
23. Søndenå, R.; Stølen, S.; Ravindran, P.; Grande, T.; Allan, N.L. Corner-versus face-sharing octahedra in $AMnO_3$ perovskites (A = Ca, Sr, and Ba). *Phys. Rev. B* **2007**, *75*, 184105. [CrossRef]
24. Kim, K.; Siegel, D.J. Correlating lattice distortions, ion migration barriers, and stability in solid electrolytes. *J. Mater. Chem. A* **2019**, *7*, 3216–3227. [CrossRef]
25. Mahana, S.; Pandey, S.K.; Rakshit, B.; Nandi, P.; Basu, R.; Dhara, S.; Turuchini, S.; Zema, N.; Manju, U.; Mahanti, S.D.; et al. Site substitution in $GdMnO_3$: Effects on structural, electronic, and magnetic properties. *Phys. Rev. B* **2020**, *102*, 245120. [CrossRef]
26. Chiang, F.K.; Chu, M.W.; Chou, F.C.; Jeng, H.T.; Sheu, H.S.; Chen, F.R.; Chen, C.H. Effect of Jahn-Teller distortion on magnetic ordering in $Dy(Fe,Mn)O_3$ perovskites. *Phys. Rev. B* **2011**, *83*, 245105. [CrossRef]
27. Cooke, A.H.; Martin, D.M.; Wells, M.R. Magnetic interactions in gadolinium orthochromite, $GdCrO_3$. *J. Phys. C Solid State Phys.* **1974**, *7*, 3133. [CrossRef]
28. Kumar, D.; Jena, P.; Singh, A.K. Structural, magnetic and dielectric studies on half-doped $Nd_{0.5}Ba_{0.5}CoO_3$ perovskite. *J. Magn. Magn. Mater.* **2020**, *516*, 167330. [CrossRef]
29. Deng, D.; Wang, X.; Zheng, J.; Qian, X.; Yu, D.; Sun, D.; Jing, C.; Lu, B.; Kang, B.; Cao, S.; et al. Phase separation and exchange bias effect in Ca doped $EuCrO_3$. *J. Magn. Magn. Mater.* **2015**, *395*, 283–288. [CrossRef]
30. Moriya, T. Anisotropic Superexchange Interaction and Weak Ferromagnetism. *Phys. Rev.* **1960**, *120*, 91–98. [CrossRef]
31. Tishin, A.M. Magnetocaloric Effect in the Vicinity of Phase Transitions. *Handb. Magn. Mater.* **1999**, *12*, 395–524. [CrossRef]
32. Lorusso, G.; Roubeau, O.; Evangelisti, M. Rotating Magnetocaloric Effect in an Anisotropic Molecular Dimer. *Angew. Chem. Int. Ed.* **2016**, *55*, 3360–3363. [CrossRef] [PubMed]
33. Landau, L.D.; Lifshitz, E.M. *Statistical Physics*; Pergamon: New York, NY, USA, 1958.
34. Amaral, V.S.; Amaral, J.S. Magnetoelastic coupling influence on the magnetocaloric effect in ferromagnetic materials. *J. Magn. Magn. Mater.* **2004**, *276*, 2104–2105. [CrossRef]